Scaling of the plasma sheath in a magnetic field parallel to the wall[a)]

Natalia S. Krasheninnikova,[b)] Xianzhu Tang, and Vadim S. Roytershteyn
Theoretical Division, Los Alamos National Laboratory, Los Alamos, New Mexico 87545, USA

(Received 30 November 2009; accepted 12 February 2010; published online 29 March 2010)

Motivated by the magnetized target fusion [R. E. Siemon *et al.*, Comments Plasma Phys. Controlled Fusion **18**, 363 (1999)] experiment, a systematic investigation of the scaling of a one-dimensional plasma sheath with a magnetic field parallel to the wall was carried out using analytical theory and the particle-in-cell code VPIC [K. J. Bowers *et al.*, Phys. Plasmas **15**, 055703 (2008)]. Starting with a uniform Maxwellian distribution in three-dimensional velocity space, plasma consisting of collisionless electrons, and ions of the same temperature interacts with a perfectly absorbing wall. A much larger ion Larmor radius causes the wall to be charged positively, creating an electric field that tends to repel the ions and attract the electrons, which is the opposite of the conventional Bohm sheath [D. Bohm, *Characteristics of Electrical Discharges in Magnetic Fields* (McGraw-Hill, New York, 1949)]. This manifests in the form of gyro-orbit modification by this spatially varying electric field, the degree of which is found to intricately depend on the relation between three parameters: electron and ion thermal Larmor radii and plasma Debye length: ρ_{the}, ρ_{thi}, and λ_D. Furthermore, the study of the sheath width scaling through the analysis of the full width at half max of electric field, x_{Eh}, elucidates three distinct types of behavior of x_{Eh}, corresponding to three different regimes: $\rho_{thi} < \lambda_D$, $\rho_{the} < \lambda_D < \rho_{thi}$, and $\lambda_D < \rho_{the}$. In addition to the sheath width, the scaling of the wall potential ϕ_{Wall}, as well as the role of the ion mass and charge Z are investigated. The results of this analytical and computational approach can also be useful in studying the plasma sheath in the conventional magnetic confinement devices, in particular at the first wall of tokamaks.
[doi:10.1063/1.3354106]

I. INTRODUCTION

Magnetoinertial fusion (MIF)[1–5] is a concept, which combines two aspects of the traditional plasma confinement techniques—magnetic and inertial, in an effort to satisfy Lawson[6] criteria for ignition. MIF operates at higher number densities than the magnetic confinement fusion requiring shorter confinement time, but not as high as the inertial confinement fusion eliminating the need for high compression ratio and speed. In particular, magnetized target fusion (MTF),[7–11] a type of MIF experiment, utilizes an imploding metal liner to compress plasma to the required ignition criteria. However, the increased number density obtained in MIF can lead to high radiation losses, an issue even at lower densities of the magnetic fusion as they degrade energy confinement and impede ignition.[12] Additionally, high Z impurities that are coming off of the impinging liner due to the plasma-surface interaction can further exacerbate the problem and cause radiation losses to be prohibitively large for MTF ignition. Therefore, it is crucial to know the impurity transport and radiation loss, of which an important part is understanding their production. As the creation of high Z impurities is governed by the plasma-surface interaction, a vital initial step is addressing the physics of such interaction.

It is well known that the plasma-surface interaction has been of great importance to the plasma physics community for a long time.[13] It applies not only to the alternative concepts such as MTF but also to such traditional topics of interest as the plasma interaction with the first wall and the divertor plates of a tokamak. Since the direct interaction of the plasma with the wall happens over a very thin layer called a sheath, understanding its behavior is essential.

Given that the plasma particles impacting the wall carry large amounts of energy, in majority of current magnetic fusion experiments with high temperature plasmas, the magnetic field is nearly aligned with the wall. This is particularly true for MTF. Therefore, understanding the physics of sheath with the magnetic field almost parallel to the wall is of great interest.

Over the past 30 years, a number of authors have examined the behavior of such a sheath,[14–28] employing a variety of analytical, computational, and experimental techniques.[26] Majority of the papers concentrated on the sheath in the regime $\rho_{the} \leq \lambda_D < \rho_{thi}$, which is relevant to the tokamak edge plasma.[14,18–20,24] Some has employed analytical formalism,[14,17–19,23,25] some fluid modeling,[20,25,28] some particle-in-cell (PIC) simulations.[19,24] A considerable amount of effort has been put into understanding such important issues as the effects of collisions,[16,18,20,21,28] atomic processes,[18,27,28] degree of magnetic field inclination,[14,15,20,21] wall roughness,[22] nonuniformity along the wall and instabilities[19] on the sheath dynamics. However, a detailed one-dimensional (1D) collisionless sheath scaling study in wide range of parameter regimes has not yet been done. The following work examines the simplest 1D collisionless sheath model, with the magnetic field strictly parallel to a perfectly absorbing wall. We present a systematic investigation of the width scaling of such a sheath with the thermal

[a)]Paper BI3 6, Bull. Am. Phys. Soc. **54**, 23 (2009).
[b)]Invited speaker.

Larmor to Debye ratio of both electrons and ions. The effects of the ion mass and charge are also investigated.

As it is well known, a conventional Bohm sheath[29–33] is formed by the motion of the lighter species, electrons, creating an electric field that attracts the ions to the wall and repels the electrons. Without collisions, the sheath width scales with Debye length. The case of the sheath with the magnetic field parallel to the wall is completely different. Its formation is caused by the motion perpendicular to the magnetic field and it is the ions, whose gyroradius is the largest between the two species (assuming similar temperatures), that charge the wall positively. This in turn creates an electric field which repels them from, and attracts the electrons to the wall. As a result, in addition to the Debye length, magnetic field brings two more characteristic length scales, electron, and ion Larmor radii, which together will play a very important role in setting the steady-state parameters of the sheath.

When the magnetic field is strong enough so that $\rho_{thi}/\lambda_D < 1$, the particles gyro-orbits are very close to being circular in the reference frame of the guiding center drift. It is rather straightforward to develop an analytical theory that describes the steady-state plasma and field profiles for the 1D case. In particular, it predicts that the full width at half max of the electric field, $x_{Eh} \approx 6.6\rho_{the}$. However, when $\vec{\mathbf{B}}$ is decreased, one has to either make certain assumptions to continue with the analytical formalism, or resort to a self-consistent simulation study that captures the physics of gyro-orbit modification by a strongly varying electric field in the sheath. Since our primary motivation is the MTF, in an effort to obtain the results that are most relevant for the experiment which has $\rho_{the}/\lambda_D \sim 1$, we proceed with the latter and utilize VPIC (Ref. 34) code. We choose a sheath model that can closely mimic the plasma conditions near the liner. Since the liner compression velocity is much slower than the ion thermal speed, it is reasonable to consider the sheath in a quasisteady-state approximation. Moreover, the MTF plasma is highly magnetized, therefore a collisionless approximation is useful. While we acknowledge that even a small amount of collisions, magnetic field inclination, wall irregularities or higher dimension can complicate the sheath dynamics, our initial goal is to thoroughly understand the basic sheath width behavior, which provides the basis to clarify these additional subtleties. Therefore, we start our simulation study by considering a 1D case, with the magnetic field parallel to a perfectly smooth absorbing wall. Much of the interesting sheath physics, e.g., scaling relations, can be clarified by contrasting the scaling behavior in the three distinct regimes of Debye length in relation to the ion and electron thermal gyroradii. Because of that, our study and the results presented here also cover the additional regimes beyond that of MTF, and would be of general interest to a high temperature plasma application, where a magnetic field aligns with a material surface.

The plan of this paper is as follows. In Sec. II, we discuss in detail the scaling of the number densities of both species for the different ratios of the thermal Larmor radius to Debye length. In Sec. III, we present a comprehensive study of the sheath width scaling through the analysis of the electric field for all ranges of ρ_{the}/λ_D ratio. We repeat the same analysis for the wall potential in Sec. IV. The effects of the ion mass and charge are discussed in Sec. V, while Sec. VI closes off with the discussion of the results and their applicability to the experiments.

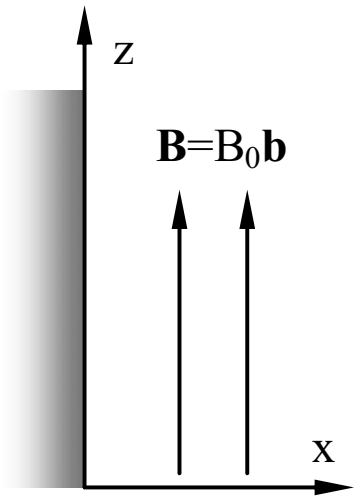

FIG. 1. Geometrical setup of 1D problem.

II. NUMBER DENSITY SCALING

In this section, we develop a framework for an analytical case of particles with circular Larmor orbits in the reference frame of the guiding center drift and compare the results with the PIC simulation using VPIC. Our analytical and simulation studies consider an initial value problem in 1D, where a collisionless plasma immersed in a magnetic field that is strictly parallel to the surface is interacting with a perfectly absorbing wall. Let the plasma consist of the electrons and ions, each initially described by a uniform Maxwellian distribution function of equal temperature

$$f_\alpha(\vec{\mathbf{x}},\vec{\mathbf{v}}) = n_0\left(\frac{m_\alpha}{2\pi T}\right)^{3/2}\exp\left[-\frac{m_\alpha(\mathrm{v}_x^2+\mathrm{v}_y^2+\mathrm{v}_z^2)}{2T}\right],$$

which is then allowed to evolve in time. The VPIC simulation captures the self-consistent formation of sheath electric field and its effects on the electron and ion gyro-orbits. If one ignores these effects that squeeze and elongate the gyro-orbits in the reference frame of the guiding center drift, an analytical calculation of the resulting particle number density profiles can be straightforwardly performed, as shown below.

Let the wall be in the y-z plane at $x=0$ and the magnetic field be uniform along the z axis: $\vec{\mathbf{B}}=B_0\hat{\mathbf{z}}=B_0\hat{\mathbf{b}}$ (see Fig. 1). The particles will gyrate around their guiding centers with the Larmor radius $\rho_L=\mathrm{v}_\perp/\omega_c$, where $\mathrm{v}_\perp=\sqrt{\mathrm{v}_x^2+\mathrm{v}_y^2}$ is the component of the velocity perpendicular to the magnetic field and $\omega_c=|q|B_0/m$ is the cyclotron frequency.

To calculate the resulting number density profile we need to establish the proper limits of integration, that is to determine exactly which particles are going to be lost to the wall based on the fact that at time $t=0$ they are located at position x with the velocity $\vec{\mathbf{v}}=\mathrm{v}_x\hat{\mathbf{x}}+\mathrm{v}_y\hat{\mathbf{y}}+\mathrm{v}_z\hat{\mathbf{z}}$. From Fig. 2 we can see that the particles, whose most left position, $x_{\min}$, is negative will impact the wall and, since it is perfectly

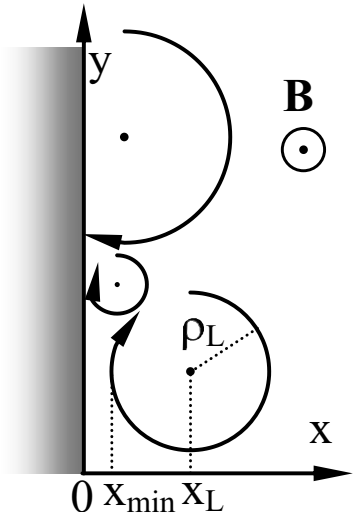

FIG. 2. Possible particle orbits in the regime of $\rho_{th} \ll \lambda_D$.

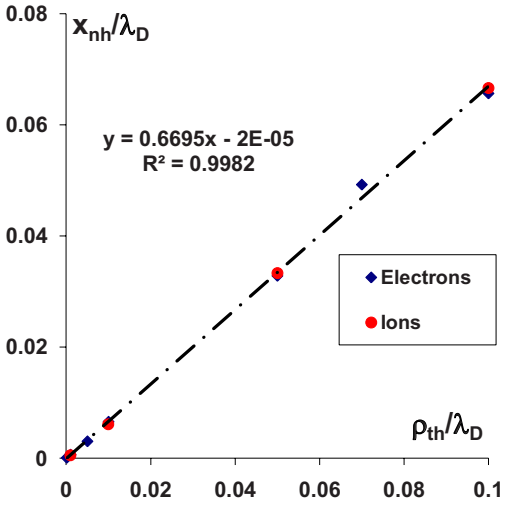

FIG. 4. (Color online) x_{nhe}/λ_D and x_{nhi}/λ_D vs their respective ρ_{th}/λ_D.

absorbing, will be lost. Thus, to calculate the number density profile we only need to integrate over the particles with $x_{\min} > 0$, where $x_{\min} = x_L - \rho_L$, $x_L = x + Zv_y/\omega_c$, $Z=1$ for ions, and $Z=-1$ for electrons, which follows from the equation of motion. The limits of integration are then given by

$$\begin{cases} Zv_y \geq -\frac{1}{2}x\omega_c \\ v_x^2 \leq x\omega_c(x\omega_c + 2Zv_y), \end{cases} \tag{1}$$

and the equilibrium number density profile is written as

$$n(\vec{x}) = \frac{n_0}{\sqrt{\pi}} \int_{-\infty}^{x/2\rho_{th}} e^{-u^2} \operatorname{erf}\left[\sqrt{\frac{x}{\rho_{th}}\left(\frac{x}{\rho_{th}} - 2u\right)} \right] du, \tag{2}$$

where $\rho_{th} = \sqrt{2T/m}/\omega_c$ and detailed calculations are left to the Appendix. The graph of such a profile, together with the simulation results for electrons and ions is given in Fig. 3 with the number density being normalized to unity. For the purposes of number density scaling, we also mark the location where the density equals to a half as x_{nh}, which from the numerical evaluation of Eq. (2) is equal to

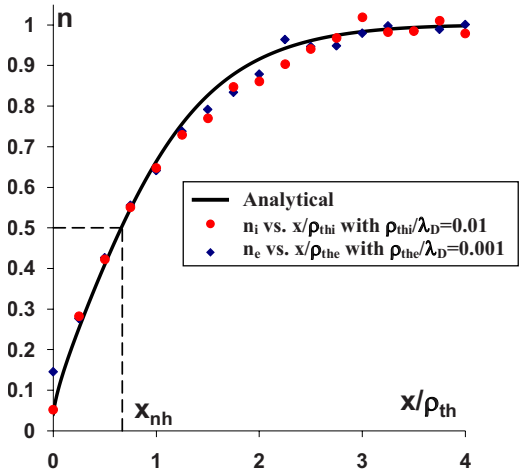

FIG. 3. (Color online) Profile of analytical number density and simulation results for ions and electrons in $\rho_{the}, \rho_{thi} \ll \lambda_D$ regime.

$$x_{nh} \approx 0.67\rho_{th}. \tag{3}$$

From the above results, we expect that when the particles respond to the electric field much slower than to $\vec{\mathbf{B}}$, the location of the half density x_{nh} for electrons and ions will be proportional to their respective ρ_{th} with the constant of proportionality being 0.67 for both species. The plasma response to the electric field is governed by the plasma frequency ω_p, while its response to the magnetic field is related to ω_c. Therefore, to confirm the results of this analytical theory we need to run the simulations in the regime $\omega_p \ll \omega_c$ or $\rho_{th}/\lambda_D \ll 1$, where λ_D is the plasma Debye length.

Using the PIC code VPIC we simulate a 1D two species hydrogen plasma with three velocity components in the regime of $\rho_{th}/\lambda_D \leq 0.1 \ll 1$. The spatial resolution is $\min(\rho_{the}, \lambda_D)/10$ and at least 4000 particles per cell are used. To speed up the calculations we employed a reduced mass so that the ratio of the ion to electron mass is $M/m = 100$ and high enough temperature so that $c/v_{the} \sim 7$, where c is the speed of light and $v_{the} = \sqrt{2T_e/m}$ is the electron thermal speed. The plots of x_{nh}/λ_D as a function of their respective ρ_{th}/λ_D are shown in Fig. 4 for the electrons and ions, where both curves have been fitted using linear regression with the goodness of fit represented by the Pearson product moment correlation coefficient—R^2 factor, which should be close to one. As we can see, the slopes for both species when plotted versus their respective thermal gyroradii are 0.67, which is in excellent agreement with the above analytical expression.

When we continue the plots in Fig. 4 to higher values of ρ_{th}/λ_D (see Fig. 5), we will observe that for the electrons, the data clearly separates into two regions: $\rho_{the}/\lambda_D < 1$ and $\rho_{the}/\lambda_D > 1$. The former is characterized by the linear dependence of x_{nhe} on ρ_{the} with the slope being very close to the earlier analytical value. The scaling in the second regime is $x_{nhe}/\lambda_D \propto 3\ln(\rho_{the}/\lambda_D)$, which indicates that the above analytical theory is no longer applicable and the effect of the electric field on the electron orbits is not negligible.

The behavior of the ion number density, shown in Fig. 6, is more complicated, as it has three distinct scaling regimes: $\rho_{thi} < \lambda_D$, $\rho_{the} < \lambda_D < \rho_{thi}$, and $\rho_{the} > \lambda_D$. The first one, just

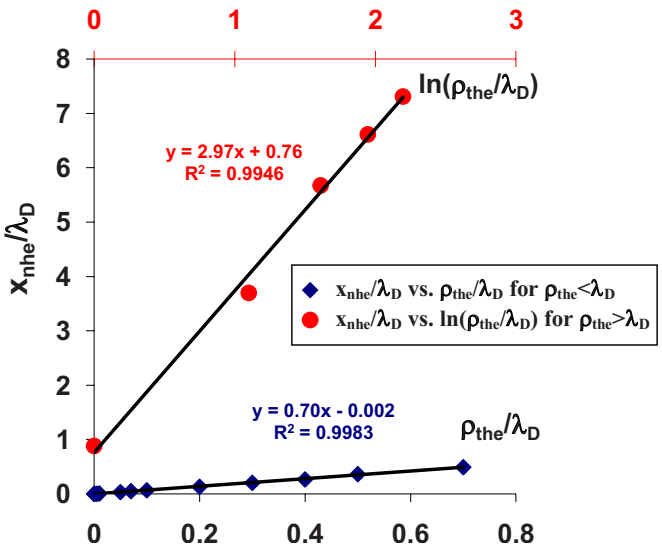

FIG. 5. (Color online) x_{nhe}/λ_D vs ρ_{the}/λ_D with linear fit in $\rho_{the}<\lambda_D$ regime and x_{nhe}/λ_D vs $\ln(\rho_{the}/\lambda_D)$ with linear fit in $\rho_{the}>\lambda_D$ regime.

like the electrons, can be described by the analytical theory, with $x_{nhi}\propto\rho_{thi}$. However, as ρ_{the}/λ_d ratio is increased, the effects of the electric field on the ions orbit cannot be ignored. The regime with $\rho_{the}>\lambda_D$ is also similar to the electrons, but the constant of proportionality is smaller: $x_{nhi}/\lambda_D\propto 2.5\ln(\rho_{thi}/\lambda_D)$. The $\rho_{the}<\lambda_D<\rho_{thi}$ regime is quite interesting, as the electrons are still on the sub-Debye scale and do not feel the presence of the ions. Their x_{nhe} still scales linearly with ρ_{the} as reflected in the previous graph for $\rho_{the}/\lambda_d\in[0.1;1]$. This regime, however, corresponds to $\rho_{thi}/\lambda_d\in[1;10]$ for the ions, which are affected by the presence of electrons, making their x_{nhi} scaling nonlinear (see Fig. 6).

When the electron Larmor radius grows to be much larger than the Debye length, it becomes more difficult to model the sheath in steady-state, as it takes much longer to achieve it and requires a much larger domain to accommodate a few ion gyroradii. If one relaxes the latter condition and allows the system size to be less than the ion Larmor radius, then the sheath reduces to the conventional one with all its classical characteristics, such as the width scaling, the velocity criterion and the wall potential.

When the system size is larger than a few ion gyroradii, before the effects of magnetic field kick in, the conventional Bohm sheath also forms. Eventually, the gyro-orbit effects become more prominent and it reverts to the sheath with the magnetic field parallel to the wall, as described above. However, as the cyclotron frequency becomes smaller, one has to re-evaluate the validity of the magnetized plasma assumptions.

III. ELECTRIC FIELD AND SHEATH WIDTH SCALING

In Sec. II, we have examined in detail the individual scaling of the electron and ion number densities, as well as their effects on each other in different regimes of the thermal Larmor to Debye ratio. In this section, we will analyze the sheath as a whole by considering the scaling of the full width at half max of the electric field, produced by the number density profiles of both species from Sec. II.

When the effects of the electric field on the particle orbits can be ignored, $\rho_{thi}\ll\lambda_D$, and the number density of each species is given by Eq. (2), the electric field for this simple 1D case can be calculated analytically using Gauss's Law, yielding

$$E_x(x) = -\frac{e}{\varepsilon_0}\int_x^\infty [n_i(x') - n_e(x')]dx'$$
$$= -\frac{n_0 e}{\sqrt{\pi}\varepsilon_0}\int_x^\infty \left\{ \int_{-\infty}^{x'/2\rho_{thi}} e^{-u^2} \times \mathrm{erf}\left[\sqrt{\frac{x'}{\rho_{thi}}\left(\frac{x'}{\rho_{thi}} - 2u\right)}\right] du - \int_{-\infty}^{x'/2\rho_{the}} e^{-u^2}\,\mathrm{erf}\left[\sqrt{\frac{x'}{\rho_{the}}\left(\frac{x'}{\rho_{the}} - 2u\right)}\right] du \right\} dx', \quad (4)$$

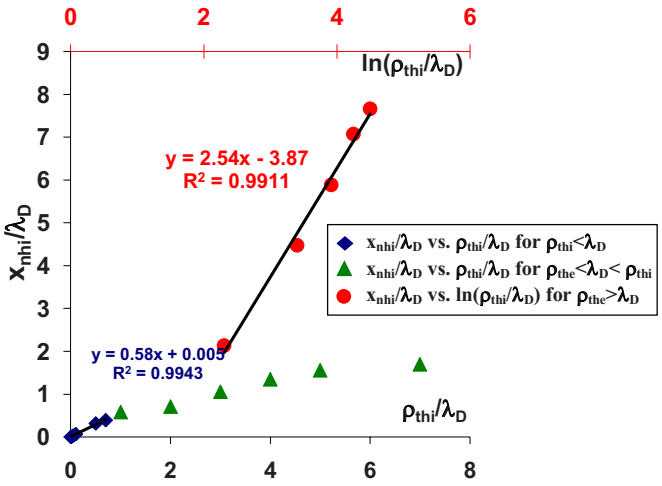

FIG. 6. (Color online) x_{nhi}/λ_D vs ρ_{thi}/λ_D in $\rho_{thi}<\lambda_D$ regime with linear fit and $\rho_{the}<\lambda_D<\rho_{thi}$ regime, x_{nhi}/λ_D vs $\ln(\rho_{thi}/\lambda_D)$ in $\lambda_D<\rho_{the}$ regime.

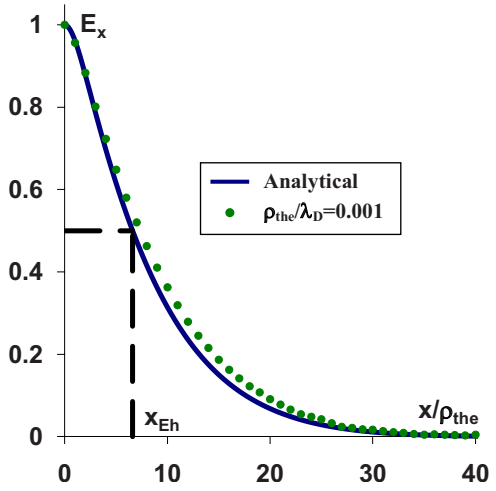

FIG. 7. (Color online) Profile of analytical 1D electric field and simulation results with $\rho_{the}/\lambda_D=0.001$.

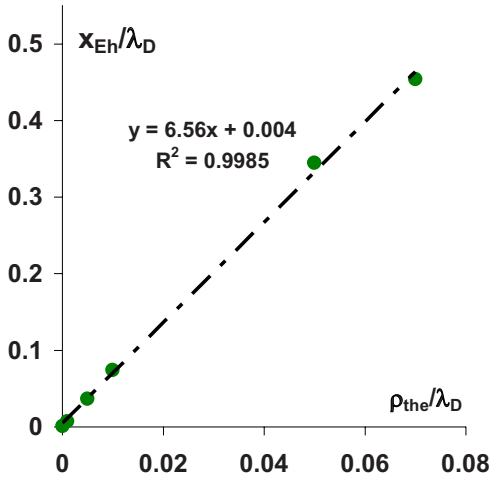

FIG. 8. (Color online) x_{Eh}/λ_D vs ρ_{the}/λ_D with linear fit in $\rho_{the},\rho_{thi} \ll \lambda_D$ regime.

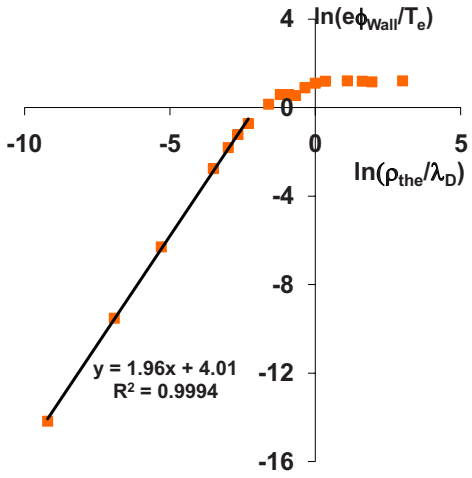

FIG. 10. (Color online) $\ln(e\phi_{\mathrm{Wall}}/T_e)$ vs $\ln(\rho_{the}/\lambda_D)$.

where we assumed that $E_x(\infty)=0$. Similar to the number density, let us introduce a measure of the sheath width, x_{Eh}, as the location of where the electric field becomes half its value at the wall, which happens to be the maximum. The plot of the normalized electric field as a function of x/ρ_{the} is given in Fig. 7. From the plot we can also see that x_{Eh} is given by

$$x_{Eh} \approx 6.60\rho_{the}. \tag{5}$$

To compare the analytical results with the VPIC simulation, we plot x_{Eh}/λ_D as a function of ρ_{the}/λ_D in the regime of $\rho_{the}/\lambda_D \leq 0.1 \ll 1$ in Fig. 8. The data is fitted to a straight line with the slope of approximately 6.56, which is in excellent agreement with the above analytical result.

When we continue the plot in Fig. 8 to higher values of ρ_{the}/λ_D, we observe that just like the ion number density, the scaling of x_{Eh} clearly separates into the same three regimes: $\rho_{thi}<\lambda_D$, $\rho_{the}<\lambda_D<\rho_{thi}$, and $\rho_{the}>\lambda_D$, see Fig. 9. In the first one $x_{Eh} \propto \rho_{the}$ and the slope agrees with the above analytical calculations. The second region also exhibits linear trend, but with a drastically different slope, indicating that the electric field cannot be described by Eq. (4). When the electron thermal Larmor radius surpasses the Debye length, the scaling changes yet again and has the form $x_{Eh}/\lambda_d \propto (\rho_{the}/\lambda_d)^p$, which is very different from our analytical results.

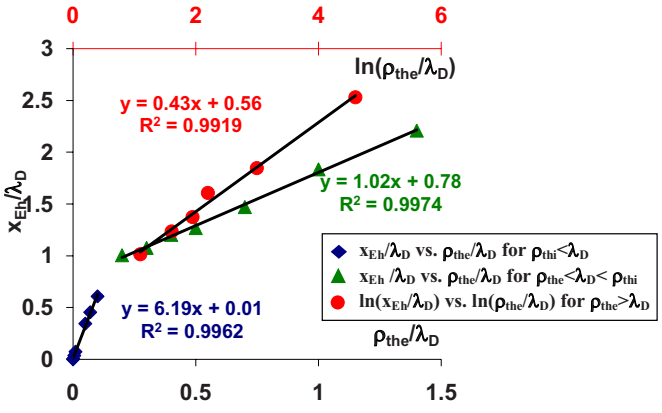

FIG. 9. (Color online) x_{Eh}/λ_D vs ρ_{the}/λ_D with linear fits in $\rho_{the}<\lambda_D$ regimes, $\ln(x_{Eh}/\lambda_D)$ vs $\ln(\rho_{the}/\lambda_D)$ with linear fit in $\rho_{the}>\lambda_D$ regime.

IV. WALL POTENTIAL

To close off our discussion about the scaling, let us look at the wall potential. In the limit of small ρ_{thi}/λ_D, we can use Eq. (4) to calculate the potential profile analytically. In particular, the wall potential in this regime is proportional to $(\rho_{the}/\lambda_D)^2$ with the constant of proportionality ~64.5. For the general case we summarize our findings by plotting $\ln(e\phi_{\mathrm{Wall}}/T_e)$ as a function of $\ln(\rho_{the}/\lambda_D)$ for a reduced ion mass of 100 in Fig. 10. From this plot we can see that when the ions are on the sub-Debye scale, that is $\rho_{thi}/\lambda_D<1$, the wall potential is proportional to the square of the electron Larmor to Debye ratio. Another feature that is also visible on this graph is that at large ratios of ρ_{the}/λ_D, the wall potential saturates at about 3.3 in the electron temperature units for $M/m=100$, while for the true hydrogen mass of $M/m=1836$, this number changes to approximately 4.

V. ION EFFECTS

As most of the results presented in the previous sections are based on the PIC simulations of the reduced ion mass of $M/m=100$, a very legitimate issue to address would be how these results change when the true hydrogen mass is considered. We summarize the results in Fig. 11 where we plot x_{Eh}/λ_D as a function of $\sqrt{M/m}$ for different values of ρ_{the}/λ_D, representing the different regimes. As it is clear from the plot, unless $\rho_{the}/\lambda_D>1$, the effect of the mass increase on the sheath scaling is rather small relative to the size of the domain, which is measured in Debye lengths. However, in the case of $\rho_{the}/\lambda_D>1$ the ion mass can make a noticeable difference, in particular when $\rho_{the}/\lambda_D=7$ the sheath width in terms of x_{Eh} has increased from approximately $3.5\lambda_D$ to $5.5\lambda_D$ when the mass was changed from $M/m=100$ to 1836.

Another interesting issue is the role of the ion charge in the sheath scaling. To address this subject, we plot $\ln(x_{Eh}/\lambda_D)$ as a function of $\ln(Z)$ in Fig. 12 for different values of ρ_{the}/λ_D, representing the different regimes. We can

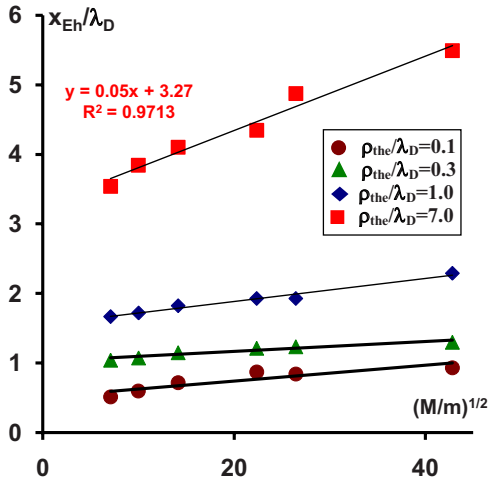

FIG. 11. (Color online) x_E/λ_D vs $(M/m)^{1/2}$ for different values of ρ_{the}/λ_D.

see that the data for the most part decreases linearly with the increasing $\ln(Z)$, indicating that $x_{Eh}/\lambda_D \propto Z^{-p}$, with p ranging from 0.5 to 0.8 depending on the regime. In particular, in the regime when both particles are on the sub-Debye scale, $p \approx 0.8$; as the ion Larmor becomes larger than the Debye length $p \approx 0.5-0.7$; and when $\rho_{the} > \lambda_D$, $p \approx 0.55$.

VI. DISCUSSION

We have examined the scaling of the sheath width through the analysis of the full width at half max of the electric field as well as the electron and ion number densities. It was found that the scaling greatly depends on the relation between three parameters: ρ_{the}, ρ_{thi}, and λ_D. In particular, three different regimes of the sheath width behavior have been identified, corresponding to $\rho_{thi} < \lambda_D$, $\rho_{the} < \lambda_D < \rho_{thi}$, and $\lambda_D < \rho_{the}$. The results in the first regime agree very well with the analytical theory presented in this paper, signifying that the particles orbits in this regime are very close to being circular and the effect of the electric field on them is negligible. While the simulation results from the middle regime cannot be described by our analytics (except for the

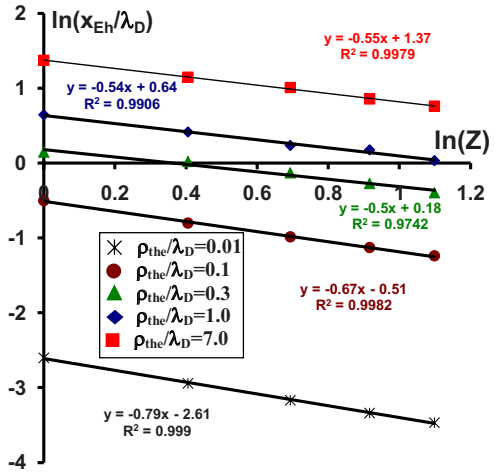

FIG. 12. (Color online) $\ln(x_{Eh}/\lambda_D)$ vs $\ln(z)$ with linear fits for different values of ρ_{the}/λ_D.

electron number density), they can be important for the tokamak divertor physics as $\rho_{the}/\lambda_D \sim 0.5$ or $n/B^2 \sim 1.25 \times 10^{18}(\mathrm{m}^{-3}/\mathrm{T}^2)$ corresponds to the typical plasma parameters there. The parameter regime in which the electron thermal Larmor radius is larger than the Debye length also has a wide range of applicability, ranging from the MTF experiment to the plasma interaction with the first wall in tokamaks.

In addition to the sheath width, the scaling of the wall potential, ϕ_{Wall}, with ρ_{the}/λ_D was investigated. The results reveal that $e\phi_{Wall}/T_e \propto (\rho_{the}/\lambda_D)^2$ in $\rho_{thi} < \lambda_D$ regime, though for large ρ_{the}/λ_D, ϕ_{Wall} saturates at around $4T_e$ for a true hydrogen plasma. The role of the ion mass and charge Z in the scaling of the sheath width was also considered. The analysis indicates that the mass can play an important role for a fixed system size when $\lambda_D < \rho_{the}$, while x_{Eh} scales very close to $1/\sqrt{Z}$ in the regimes of most interest to experiments.

ACKNOWLEDGMENTS

This research was supported by the LDRD-ER (Project No. 20090410ER) *"Transport in Magnetized Dense Plasmas for Magneto-Inertial Fusion"* at the Applied Mathematics and Plasma Theory group of Theoretical Division of Los Alamos National Laboratory. The authors are extremely grateful to Kevin Bowers, Brian Albright, and the rest of the VPIC team for making their code available to us for this work. We are also indebted to the Institutional Computing team at LANL, particularly Robert Tomlinson for providing us with the allocation on Coyote cluster.

APPENDIX: ANALYTICAL NUMBER DENSITY

The equation of motion for the particle in a uniform constant magnetic field is

$$\begin{cases} x_p(t) = x_L - Z\rho_L \cos(\omega_c t + \theta) \\ \mathrm{v}_y(t) = \rho_L \omega_c \cos(\omega_c t + \theta) = \mathrm{v}_\perp \cos(\omega_c t + \theta). \end{cases}$$

At $t=0$ $x_p(0) \equiv x = x_L - Z\rho_L \cos\theta$ and $\mathrm{v}_y(0) \equiv \mathrm{v}_y = \mathrm{v}_\perp \cos\theta$. The condition for the particles to contribute to the number density is $x_L - \rho_L \geq 0$. Substituting the previous expressions into this inequality yields

$$x_L \omega_c = x\omega_c + Z\mathrm{v}_y \geq \rho_L \omega_c = \mathrm{v}_\perp \geq 0,$$

$$(x\omega_c + Z\mathrm{v}_y)^2 \geq \mathrm{v}_\perp^2 = \mathrm{v}_x^2 + \mathrm{v}_y^2 \geq 0,$$

$$x\omega_c(x\omega_c + 2Z\mathrm{v}_y) \geq \mathrm{v}_x^2 \geq 0.$$

Therefore, the limits of integration for the distribution function should be

$$\begin{cases} Z\mathrm{v}_y \geq -\frac{1}{2} x\omega_c \\ \mathrm{v}_x^2 \leq x\omega_c(x\omega_c + 2Z\mathrm{v}_y). \end{cases}$$

The particle number density for the electrons can therefore be calculated as

$$n_e(\vec{\mathbf{x}},t)=\int f_e(\vec{\mathbf{x}},\vec{\mathbf{v}},t)d\vec{\mathbf{v}}=n_0\left(\frac{m}{2\pi T}\right)^{3/2}\int_{-\infty}^{+\infty}e^{-m\mathrm{v}_z^2/2T}d\mathrm{v}_z\int_{-\infty}^{+x\omega_{ce}/2}d\mathrm{v}_y e^{-m\mathrm{v}_y^2/2T}\left(\int_{-\sqrt{x\omega_{ce}(x\omega_{ce}-2\mathrm{v}_y)}}^{+\sqrt{x\omega_{ce}(x\omega_{ce}-2\mathrm{v}_y)}}e^{-m\mathrm{v}_x^2/2T}d\mathrm{v}_x\right)$$

$$=\frac{n_0}{\sqrt{\pi}}\int_{-\infty}^{+x/2\rho_{the}}e^{-\mathrm{u}^2}\,\mathrm{erf}\left[\sqrt{\frac{x}{\rho_{the}}\left(\frac{x}{\rho_{the}}-2u\right)}\right]d\mathrm{u},$$

and similarly for the ions

$$n_i(\vec{\mathbf{x}},t)=\int f_i(\vec{\mathbf{x}},\vec{\mathbf{v}},t)d\vec{\mathbf{v}}=n_0\left(\frac{M}{2\pi T}\right)^{3/2}\int_{-\infty}^{+\infty}e^{-M\mathrm{v}_z^2/2T}d\mathrm{v}_z\int_{-x\omega_c/2}^{+\infty}d\mathrm{v}_y e^{-M\mathrm{v}_y^2/2T}\left(\int_{-\sqrt{x\omega_{ci}(x\omega_{ci}+2\mathrm{v}_y)}}^{+\sqrt{x\omega_{ci}(x\omega_{ci}+2\mathrm{v}_y)}}e^{-M\mathrm{v}_x^2/2T}d\mathrm{v}_x\right)$$

$$=\frac{n_0}{\sqrt{\pi}}\int_{-x/2\rho_{thi}}^{+\infty}e^{-\mathrm{u}^2}\,\mathrm{erf}\left[\sqrt{\frac{x}{\rho_{thi}}\left(\frac{x}{\rho_{thi}}+2u\right)}\right]d\mathrm{u}=\frac{n_0}{\sqrt{\pi}}\int_{-\infty}^{+x/2\rho_{thi}}e^{-\mathrm{u}^2}\,\mathrm{erf}\left[\sqrt{\frac{x}{\rho_{thi}}\left(\frac{x}{\rho_{thi}}-2u\right)}\right]d\mathrm{u}.$$

[1] A. E. Robson and P. J. Turchi, *Pulsed High Beta Plasmas*, Third Topical Conference on Pulsed High Beta Plasmas (Pergamon, New York, 1976), p. 477.
[2] P. J. Turchi, *Review on the NRL Liner Implosion Program*, Magagauss Physics and Technology (Plenum, New York, 1980), p. 375.
[3] I. R. Lindermuth and M. M. Widner, Phys. Fluids **24**, 753 (1981).
[4] I. R. Lindermuth and R. C. Kirkpatrick, Nucl. Fusion **23**, 263 (1983).
[5] C. J. Keane, D. Kovar, and Y. C. F. Thio, *Report of the Interagency Task Force on High Energy Density Physics* (National Science and Technology Council, Committee on Science, OSTP, Washington, DC, 2007).
[6] J. D. Lawson, Proc. Phys. Soc. London, Sect. B **70**, 6 (1957).
[7] R. C. Kirkpatrick, I. R. Lindemuth, and M. S. Ward, Fusion Technol. **27**, 201 (1995).
[8] R. P. Drake, J. Hammer, C. Hartman, J. Perkins, and D. D. Ryutov, Fusion Technol. **30**, 310 (1996).
[9] G. A. Wurden, K. F. Schoenberg, and R. E. Siemon, J. Plasma Fusion Res. SERIES **2**, 238 (1999).
[10] R. E. Siemon, I. R. Lindermuth, and K. F. Schoenberg, Comments Plasma Phys. Controlled Fusion **18**, 363 (1999).
[11] T. Intrator, S. Y. Zhang, J. H. Degnan, I. Furno, C. Grabowski, S. C. Hsu, E. L. Ruden, P. G. Sanchez, J. M. Taccetti, M. Tuszewski, W. J. Waganaar, and G. A. Wurden, Phys. Plasmas **11**, 2580 (2004).
[12] ITER Physics Basis, Nucl. Fusion **39**, 2209 (1999).
[13] R. N. Franklin, J. Phys. D **36**, R309 (2003).
[14] U. Daybelge and B. Bein, Phys. Fluids **24**, 1190 (1981).
[15] R. Chodura, Phys. Fluids **25**, 1628 (1982).
[16] J. Behnel, Ph.D. thesis, Ruhr Universitate Bochum, 1985.
[17] R. D. Hazeltine, Phys. Fluids B **1**, 2031 (1989).
[18] M. J. Gerver, S. E. Parker, and K. Theilhaber, Phys. Fluids B **2**, 1069 (1990).
[19] K. Theilhaber and C. K. Birdsall, Phys. Fluids B **1**, 2244 (1989).
[20] D. L. Holland, B. D. Fried, and G. L. Morales, Phys. Fluids B **5**, 1723 (1993).
[21] K.-U. Riemann, Phys. Plasmas **1**, 552 (1994).
[22] R. H. Cohen and D. D. Ryutov, Phys. Plasmas **5**, 2194 (1998).
[23] P. C. Stangeby, *The Plasma Boundary of Magnetic Fusion Devices* (IOP, Bristol, 2000).
[24] D. Tskhakaya and S. Kuhn, Contrib. Plasma Phys. **44**, 564 (2004).
[25] N. Sternberg and J. Poggie, IEEE Trans. Plasma Sci. **32**, 2217 (2004).
[26] N. Hershkowitz, Phys. Plasmas **12**, 055502 (2005).
[27] D. Tskhakaya, S. Kuhn, Y. Tomita, K. Matyash, R. Schneider, and F. Taccogna, Contrib. Plasma Phys. **48**, 121 (2008).
[28] D. Tskhakaya, P. K. Shukla, B. Eliasson, and S. Kuhn, Phys. Plasmas **12**, 103503 (2005).
[29] I. Langmuir, Gen. Electr. Rev. **26**, 731 (1923).
[30] I. Langmuir, Proc. Natl. Acad. Sci. U.S.A. **14**, 627 (1928).
[31] L. Tonks and I. Langmuir, Phys. Rev. **34**, 876 (1929).
[32] D. Bohm, *Characteristics of Electrical Discharges in Magnetic Fields* (McGraw-Hill, New York, 1949).
[33] A. Kono, J. Phys. D **37**, 1945 (2004).
[34] K. J. Bowers, B. J. Albright, L. Yin, B. Bergen, and T. J. T. Kwan, Phys. Plasmas **15**, 055703 (2008).